Coordinated Control of Energy Storage in Networked Microgrids under Unpredicted Load Demands

Md Tanvir Arafat Khan, *Student Member, IEEE,* Rafael Cisneros, Aranya Chakrabortty, *Senior Member, IEEE,*
Iqbal Husain, *Fellow, IEEE*

Abstract—In this paper a nonlinear control design for power balancing in networked microgrids using energy storage devices is presented. Each microgrid is considered to be interfaced to the distribution feeder though a solid-state transformer (SST). The internal duty cycle based controllers of each SST ensures stable regulation of power commands during normal operation. But problem arises when a sudden change in load or generation occurs in any microgrid in a completely unpredicted way in between the time instants at which the SSTs receive their power setpoints. In such a case, the energy storage units in that microgrid must produce or absorb the deficit power. The challenge lies in designing a suitable regulator for this purpose owing to the nonlinearity of the battery model and its coupling with the nonlinear SST dynamics. We design an input-output linearization based controller, and show that it guarantees closed-loop stability via a cascade connection with the SST model. The design is also extended to the case when multiple SSTs must coordinate their individual storage controllers to assist a given SST whose storage capacity is insufficient to serve the unpredicted load. The design is verified using the IEEE 34-bus distribution system with nine SST-driven microgrids.

Index Terms—Solid-state transformer, microgrid, energy storage, power sharing.

I. INTRODUCTION

IN recent years power engineers have started visiting the concept of networked microgrids [1], [2], where individual microgrids are coordinated to create convenient electrical topologies that guarantee reliable flow of power from one part of the grid to another, especially during emergency scenarios. An excellent resource for sensing and controlling such power flows is a solid-state transformers (SST) [3]. A schematic diagram of a radially networked microgrid, where each individual microgrid is interfaced with the distribution feeder through a SST, is shown in Fig 1. The SST consists of three power electronic converter stages—namely, rectifier, dual-active bridge, and inverter, which in turn are connected to AC and DC generators (for example, wind and solar PV), AC and DC loads, and most importantly a DC energy storage. The circuit diagram of a SST with these three stages is shown in Fig. 2.

Power balancing mechanisms for these types of networked systems typically consist of two steps. First, a supervisory controller, commonly referred to as an intelligent energy

management (IEM) at the distribution substation, predicts the load for each microgrid fifteen to twenty minutes ahead of time, solves power flow, and generates the voltage and current setpoints for each SST. When the loads change at the scheduled instants of time, the internal duty cycle based controller in the rectifier circuit of the SST (referred to as an intelligent power management (IPM) controller) gets triggered, and drives the steady-state voltages and currents to the respective setpoints using available power generation from wind and solar PV. A challenge, however, arises when any load changes significantly in between the scheduled instants of IEM commands in an unforeseen and unpredicted way. In such a case, the battery of the SST must instantaneously trigger to produce or absorb the deficit power. Appropriate control systems with fast tracking properties need to be designed for this purpose. While several papers in recent literature have reported such battery controls [4]–[6], most of them are based on simplified linear (or linealized) models of batteries that lack analytical guarantees of stability margins that can be achieved in realistic nonlinear models. Moreover, when the energy storage system is connected to the rest of the microgrid, the nonlinear dynamics coupling both may be a source of instability as well. Therefore, stable operation of the entire microgrid needs to be established. The problem becomes even more complicated when multiple microgrids need to coordinate the control actions to serve a given SST whose storage capacity is insufficient to serve its unpredicted load.

In this paper, a nonlinear control design is proposed for solving this tracking control problem. Each energy storage unit is operated in controlled-current mode with its reference current set such that the deficit power between generation and load is driven to zero autonomously within each microgrid, thereby maintaining power balance in the network.When the deficit cannot be autonomously supported, balance is maintained collectively via co-ordination between the battery controllers. Since it allows for regulation of power flows in each microgrid, the proposed control scheme may be viewed either as *tertiary* control following the terminology used in [1], or *secondary* control following that in [7]. Furthermore, the controller is based on the input-output linearization method [13]. This control technique allows us to achieve an exponentially stable tracking error. It is shown that the system, however, is not completely input-output feedback linearizable as a result of which the stability of the residual dynamics needs to be established. It is proved
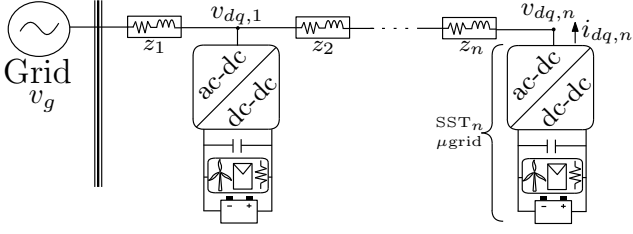
Fig. 1: Radial topology: each SST-driven microgrid is composed of renewable resources, an energy storage unit and a load.

Fig. 2: SST based distribution system.

that the currents and the voltages of the SST remain bounded while the tracking error goes to zero. Also, the margins are provided for the stable operation of each storage unit. Finally, the stability proof is extended to the multiple SST case. Power sharing algorithms are also provided for situations where the slack created from the load in one microgrid can be cooperatively fulfilled. The rest of the paper is structured as follows. In Section II, the model of a SST driven microgrid is provided. In Section III, the proposed controller is derived and the stable operation of the closed-loop is proven for the multi-SST system. In Sections IV and V, power sharing methods are introduced. Section VI assesses the proposed controller using a nine-SST distribution system. Conclusions are drawn in Section VI.

II. MICROGRID MODEL OF THE SST-DRIVEN SYSTEM

The microgrid model for our study is considered to be interfaced with the distribution feeder through a SST, as shown in Fig. 1. We consider operation of the microgrid in grid-connected mode, whereby the d and q axes voltages of the grid v_d and v_q act as excitation sources for the SST circuit, as shown in Fig. 2. Each SST consists of a front-end rectifier stage, which converts high voltage AC to high voltage DC, a dual-active bridge (DAB) stage, which
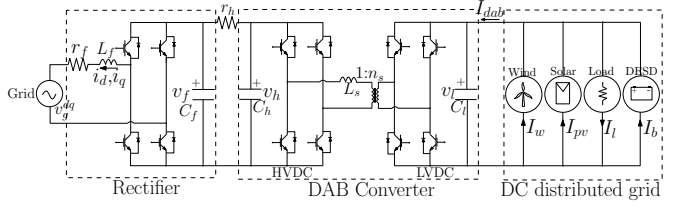
converts high DC voltage to a low DC voltage to be used for DC distribution segment, and a voltage-source inverter, which converts low DC voltage to low single-phase AC voltage to be used for AC distribution segments [8]. The rectifier is responsible for maintaining the high voltage (HV) DC—i.e., the input voltage of the DAB stage. The DAB converter regulates the low voltage (LV) DC bus. Wind power generators, solar/photovoltaic generators, loads, and an energy storage unit are assumed to be connected at the back-end of the SST. Since storage will always be connected to the DC bus, the inverter stage of the SST is not considered in the present study. Also, the network consist of n microgrids connected over a radial topology, as shown in Fig. 1—see also [9]. In the following, we briefly recall the state equations for each SST stage, keeping details to only as much as we would need to design our controller in Section III.

A. Rectifier

The dq-dynamics of the rectifier in the ith SST (for $i = 1, \cdots, n$) are[1]

$$\dot{i}_{di} = -\frac{r_{fi}}{L_{fi}} i_{di} + \omega_i i_{qi} + \frac{1}{L_{fi}} d_{1i} v_{fi} - \frac{1}{L_{fi}} v_{di} \quad (1)$$

$$\dot{i}_{qi} = -\omega_i i_{di} - \frac{r_{fi}}{L_{fi}} i_{qi} + \frac{1}{L_{fi}} d_{2i} v_f - \frac{1}{L_{fi}} v_{qi} \quad (2)$$

$$\dot{v}_{fi} = -\frac{1}{2C_{fi}}(d_{1i} i_{di} + d_{2i} i_{qi}) - \frac{v_{fi} - v_{hi}}{C_{fi}} + \frac{1}{C_{fi}}(d_{1i} i_{di} + d_{2i} i_{qi}) \cos 2\theta_i + \frac{1}{C_{fi}}(d_{1i} i_{qi} + d_{2i} i_{di}) \sin 2\theta_i \quad (3)$$

$$\dot{\xi}_{1i} = v_{fi}^\star - v_{fi} \quad (4)$$

$$\dot{\xi}_{2i} = k_{1i}(v_{fi}^\star - v_{fi}) + k_{2i}\xi_{1i} - i_{di} \quad (5)$$

$$\dot{\xi}_{3i} = i_{qi}^\star - i_{qi} \quad (6)$$

where

$$v_{di} = v_g^d + r_i \sum_{j=1}^n i_{dj} - x_i \sum_{j=1}^n i_{qj} \quad (7)$$

$$v_{qi} = v_g^q + r_i \sum_{j=1}^n i_{dj} + x_i \sum_{j=1}^n i_{qj} \quad (8)$$

and

$$d_{1i} = k_{4i}[k_{1i}(v_{fi}^\star - v_{fi}) + k_{2i}\xi_{1i} - i_{di}] + k_{3i}\xi_{2i}, \quad (9)$$

$$d_{2i} = k_{5i}(i_{qi}^\star - i_{qi}) + k_{6i}\xi_{3i}. \quad (10)$$

The physical meanings of all the states and parameters are listed in Table I. Here, v_g^d and v_g^q are the d-axis and q-axis

TABLE I: Nomenclature

System Variables					
	Rectifier		DAB Converter		Storage
i_d, i_q	d, q-axis current	v_h	High voltage bus	v_{in}	Conv. input volt.
v_f	Filter cap. volt.	v_l	Low voltage bus	v_o	Conv. outp. volt.
ξ_1, ξ_2	Voltage control	ξ_4	Low voltage ctrl.	v_b	Battery voltage
ξ_3	q-axis control	I_{dab}	Net μgrid current	ϕ	Conv. phase shift
d_1	d-axis crtl. input	ϕ_s	Phase shift ratio	I_b	Output current
d_2	q-axis ctrl. input				

System Parameters					
	Rectifier		DAB Converter		Storage
C_f	Filter capacitor	C_h	High volt. cap.	C_{in}	Conv. input cap.
L_f	Filter inductor	L_s	Transf. inductor	C_o	Conv. output cap.
r_f	Filter resistor	C_l	Low volt. cap.	L_b	Conv. transf. ind.
k_1-k_6	Controllers gains	r_h	Input resistor	r_{in}	Input resistance
ω	Line frequency	n_s	Transf. ratio	r_o	Output resistance
		f_s	Switch. freq.	n_b	Conv. transf. ratio
		k_7, k_8	Controllers gains	f_b	Switch. freq.

System References					
	Rectifier		DAB Converter		Storage
$i_d^\star, i_q^\star$	d, q-axis current	$v_l^\star$	Low DC voltage	I_b^r	Output current
$i_f^\star$	DC rect. voltage				

[1]To avoid stacking, the argument t in time-varying variables is omitted when clear from the context.

input grid voltage, $z_i = r_i + jx_i$ is the line impedance linking the ith SST to its aforegoing neighbor (see Fig. 1).

B. Dual Active Bridge Converter

The second stage of a SST is the dual-active bridge (DAB) DC-DC converter. A controller is used to regulate the output voltage of the DAB to its desired value by controlling the phase shift via switching of two H-bridges [10], [11]. The state-space representation of this stage can be written as

$$\dot{v}_{hi} = \frac{v_{fi} - v_{hi}}{C_{hi}r_{hi}} - \frac{n_{si}\phi_{si}(1 - \phi_{si})}{2C_{hi}f_i L_{si}}v_{li}, \quad (11)$$

$$\dot{v}_{li} = \frac{n_{si}\phi_{si}(1 - \phi_{si})}{2C_{li}f_{si}L_{si}}v_{hi} - \frac{I_{dabi}}{C_{li}}, \quad (12)$$

$$\dot{\xi}_{4i} = v_{li}^{\star} - v_{li}. \quad (13)$$

The control input for DAB is the phase shift ratio ϕ_{si}, designed using a PI controller as

$$\phi_{si} = k_{7i}(v_{li}^{\star} - v_{li}) + k_{8i}\xi_{4i}. \quad (14)$$

C. DC Distributed Renewable Energy Sources

The wind and solar generators, connected to the DC bus, are modeled as current sources $I_w(t)$ and $I_{pv}(t)$ as shown in Fig 2. Similarly, the load is modeled as constant current $I_l(t)$. Further details on dynamic modelling of renewable sources in a SST-based microgrid appear in [9].

D. DC Distributed Energy Storage Devices (DESD)

A DESD is made of two interconnected units: a battery energy storage and an interfacing power converter. The battery is a complex electrochemical system whose equivalent electrical circuit models are widely available in the literature (see for example [12] and the references therein). Since, the battery can consume or dispatch power, a bidirectional DC-DC converter is needed to integrate the storage to the DC bus. The DAB converter in (11)-(12) can be used for this task. The resulting DESD system is depicted in Fig. 3. Its model equations are

$$\dot{v}_o = \frac{1}{r_o C_o}(v_l - v_o) - \frac{u_b}{C_o}v_{in}, \quad (15)$$

$$\dot{v}_{in} = \frac{v_b - v_{in}}{C_{in}r_{in}} - \frac{u_b}{C_{in}}v_o \quad (16)$$

where

$$u_b := \frac{\phi_b(1 - \phi_b)n_b}{2f_b L_b}. \quad (17)$$

and ϕ_b is the phase shift ratio which acts as the control input of the converter. The input signal $\phi_b \in [-1, 1]$, i.e., it has a limited range of operation. Equations (15)-(17) denote the DESD model for the ith SST, but for simplicity we have dropped the subscript i. This slight abuse of notation will be followed in the forthcoming sections also whenever the subscript is clear from the context to avoid overuse of notations.

The output current of the storage I_b, shown in Fig. 2 and 3, can be written as

$$I_b = \frac{1}{r_o}(v_o - v_l). \quad (18)$$

The battery voltage v_b is always positive. The battery management system (BMS) supervises the appropriate operation of the battery currents and voltages. Protection hardware limits the battery operation to avoid damage of the equipment when is required by the BMS. Thus, for the rest of the paper we make the following practical assumption:

Assumption 1: Voltage $v_b \in \mathbb{R}_{>0} \cap \mathcal{L}_\infty$ with $v_b \in [v_b^{min}, v_b^{max}]$.

In the following sections, an isolated DC-DC converter will be used as the interfacing device between the voltage v_l and the voltage of the DC-link for simplicity. An analogous control design and stability proof can be derived if a non-isolated converter is used.

III. DESD CONTROL DESIGN AND STABILITY PROOF

A schematic digram for the operation of the overall networked microgrid is shown in Fig. 4. In practice, a supervisory controller predicts the load for each microgrid 15-20 minutes ahead of time, solves power flow, and generates the power setpoints $P_{rec}^{\star}$ for each SST. However, problem arises when an unpredicted load change occurs in between the scheduled instants. When that happens, the storage unit of the SST must trigger to produce or absorb the deficit power so that the power balance is maintained. The setpoints in this case are calculated in accordance with the capacity of every storage unit from a power sharing algorithm which will be provided shortly in Section IV.

By regulating I_{dab}, the proposed design permits to control the power flow between the microgrid and the transmission grid. This can be viewed as tertiary control following [1], or secondary control following [7]. Once $P_{rec}^{\star}$ is scheduled by the power sharing algorithm, the control objective is to regulate the DC grid current I_{dab} to

$$I_{dab}^{\star} = \frac{1}{v_l^{\star}}\left[P_{rec}^{\star} - \frac{(v_f^{\star} - v_h^{\star})^2}{r_h}\right]. \quad (19)$$

This function is denoted as the 'F(·)' block in Fig. 4. Using KCL from Fig. 2,

$$I_{dab}(t) = I_{pv}(t) + I_w(t) + I_b(t) - I_l(t) \quad (20)$$

which in steady-state operation becomes

$$I_{dab}^{\star} = I_{pv}(t) + I_w(t) + I_b^r(t) - I_l(t), \quad (21)$$

where $I_b^r(t)$ is the storage output reference current needed to maintain $I_{dab} = I_{dab}^{\star}$. Subtracting (21) to (20) yields

$$I_b^r(t) = I_b(t) - I_{dab}(t) + I_{dab}^{\star}. \quad (22)$$

Thus, the controller objective is:
C1. To drive the current $I_b(t)$ to $I_b^r(t)$—see Section III-B.
C2. To guarantee stable operation of the entire SST network, i.e., the interconnected dynamic system (1)-(17) for $i = 1, .., n$—see Section III-C.

A. Control design

The controller design is presented in this section based on input-output (partial) linearization [13]. As a first step, we define the tracking error δ

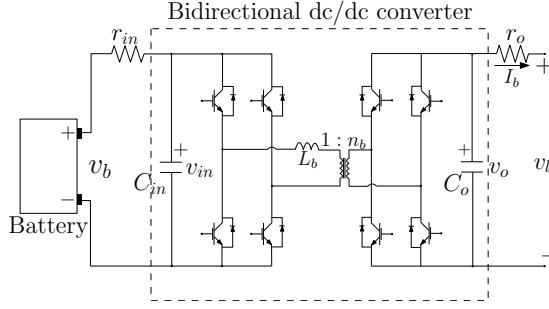$$\delta = I_b - I_b^r = \frac{v_o - v_l}{r_o} - I_b^r. \quad (23)$$

Fig. 3: DC DESD circuit.

Fig. 4: Multi-SST power sharing and energy storage control

Then, using (16) the time-derivative of δ is

$$\dot{\delta} = \frac{1}{r_o}(\dot{v}_o - \dot{v}_l) - \dot{I}_b^r$$

$$= \frac{1}{r_o^2 C_o}(v_l - v_o) + \frac{1}{r_o C_o}v_{in}u_b - \frac{\dot{v}_l}{r_o} - \dot{I}_b^r. \quad (24)$$

To assign an exponentially convergent error in closed-loop, the right-hand side of the last expression is equated to a scaling term of δ:

$$-\frac{\kappa_p}{r_o C_o}\delta = -\frac{\kappa_p}{r_o C_o}\left(\frac{v_o - v_l}{r_o} - I_b^r\right),$$

where (free) gain $\kappa_p > 0$. Doing so, one gets

$$\frac{1}{r_o^2 C_o}(v_l - v_o) + \frac{1}{r_o C_o}v_{in}u_b$$
$$-\frac{\dot{v}_l}{r_o} - \dot{I}_b^r = -\frac{\kappa_p}{r_o C_o}\left(\frac{v_o - v_l}{r_o} - I_b^r\right).$$

From the last equation

$$u_b = \frac{1}{v_{in}}\left[\frac{1}{r_o}(1 - \kappa_p)(v_o - v_l) + \kappa_p I_b^r\right.$$
$$\left. + r_o C_o \dot{I}_b^r + C_o \varphi_{v_l}(t)\right], \quad (25)$$

with function $\varphi_{v_l}(t) := \dot{v}_l(t)$, i.e., where the expression for $\dot{v}_l$ follows from the RHS of (12).

Note that although u_b is chosen as the designable control input in (25), the actual control input to the system is the phase shift ϕ_b. Thus, with u_d as in (25), it is necessary to obtain the inverse mapping of (17). Since the duty cycle u_b is always bounded within $[-1, 1]$, from the quadratic equation (17) it follows that ϕ_b is given by the piecewise function

$$\phi_b = \begin{cases} -\frac{1}{2} \pm \frac{1}{2}\sqrt{1 - 4h} & u_b \in [0, \frac{n_b}{8f_b L_b}] \\ -\frac{1}{2} - \frac{1}{2}\sqrt{1 - 4h} & u_b \in [-\frac{n_b}{f_b L_b}, 0], \end{cases} \quad (26)$$

with $h := \frac{2f_b L_b}{n_b}u_b$.

B. Stability of the DESD system

Note that the DESD system (15)-(16) has relative degree one with respect to δ, i.e., the system is not fully feedback linearizable. Therefore, stability of the residual dynamics has to be proven. This is addressed in the next proposition. Before proceeding, we make the following practical assumption.

Assumption 2: Signals I_b^r and $\dot{I}_b^r$ are bounded and, for any operation around the equilibrium point, v_l and φ_{v_l} are also bounded for all $t \geq 0$.
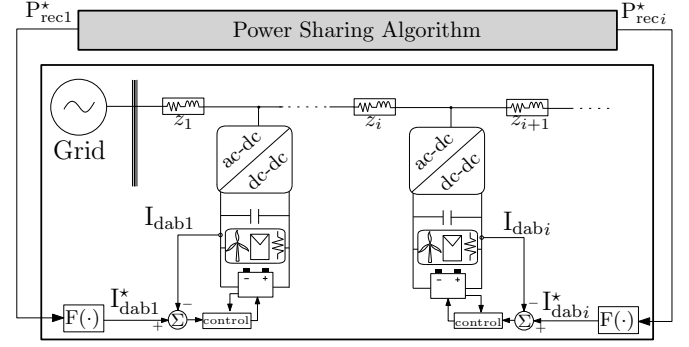
Boundedness of v_l and φ_{v_l} will follow from the stability proof of the multi-SST system, provided in Section III-C. At this point this is taken as an assumption to proceed with Proposition 1. Boundedness of the generation and load currents I_w, I_{pv} and I_l follows from the physics. Thus, using (21), I_b^r is also bounded. Finally, since high frequencies in I_b^r are filtered out when implementing (see Fig. 6), it is reasonable to consider $\dot{I}_b^r$ to be bounded as well.

Proposition 1: Consider the system (15)-(16) in closed-loop with (25). Define

$$p(t) := v_o\left[\frac{1}{r_o}(1 - \kappa_p)(v_o - v_l) + \kappa_p I_b^r + r_o C_o \dot{I}_b^r + C_o \varphi_{v_l}\right].$$

Then,

P1. The tracking error δ is exponentially stable with

$$\delta(t) = \lim_{t \to \infty} \delta(0)\exp\left(-\frac{\kappa_p}{r_o C_o}t\right).$$

P2. There exists a bound $|p(t)| \leq p_{max}$ such that for all initial conditions $(v_o(0), v_{in}(0)) \in \mathbb{R}^2$ with

$$v_{in}(0) > \frac{1}{2}v_b^{min} - \frac{1}{2}\sqrt{(v_b^{min})^2 - 4C_{in}p_{max}}$$

with $(v_b^{min})^2 - 4C_{in}p_{max} \geq 0$, voltages v_o and v_{in} remains bounded. Moreover, there exist parameters f_b, L_b and n_b such that

$$u_b \in \left[-\frac{n_b}{f_b L_b}, \frac{n_b}{8f_b L_b}\right]. \quad (27)$$

Proof. The closed-loop system is formed by the error dynamics together with (16) taking u_b as in (25). Thus,

$$\dot{\delta} = -\frac{\kappa_p}{r_o C_o}\delta \quad (28)$$

$$\dot{v}_{in} = -\frac{v_{in}}{r_{in}C_{in}} - \frac{p(t)}{C_{in}v_{in}} + \frac{v_b}{r_{in}C_{in}}. \quad (29)$$

Since (28) is decoupled from (29), P1 immediately follows. Next, using (23) one can conclude boundedness of v_o and, from Assumption 2, the existence of bound p_{max} in $p(t)$. For $v_{in} > 0$,

$$\Phi_{min}(v_{in}) \leq \dot{v}_{in} \leq \Phi_{max}(v_{in})$$

where

$$\Phi_{min}(v_{in}) := -\frac{v_{in}}{r_{in}C_{in}} - \frac{p_{max}}{C_{in}v_{in}} + \frac{v_b^{min}}{r_{in}C_{in}} \quad (30)$$
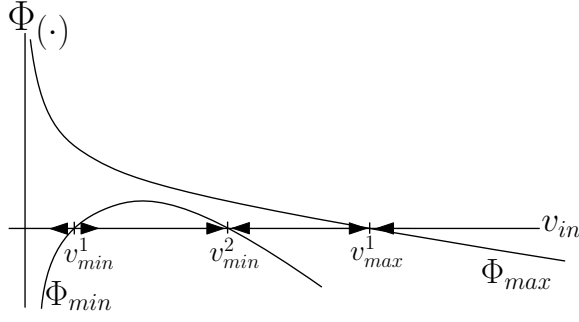
Fig. 5: Plot of v_{in} vs. Φ_{max}, Φ_{min}

Fig. 6: Implementation diagram for the proposed DESD controller

$$\Phi_{max}(v_{in}) := -\frac{v_{in}}{r_{in}C_{in}} + \frac{p_{max}}{C_{in}v_{in}} + \frac{v_b^{max}}{r_{in}C_{in}} \qquad (31)$$

and constants $v_b^{min}, v_b^{max} > 0$ follows from Assumption 1. The corresponding plots are depicted in Fig. 5. The points v_{min}^1 and v_{min}^2 correspond to the roots of (30), and v_{max}^1 corresponds to the positive root of (31). Thus,

$$
\begin{aligned}
v_{min}^{1,2} &= \frac{1}{2}v_b^{min} \pm \frac{1}{2}\sqrt{(v_b^{min})^2 - 4C_{in}p_{max}} \\
v_{max}^1 &= \frac{1}{2}v_b^{min} + \frac{1}{2}\sqrt{(v_b^{min})^2 + 4C_{in}p_{max}}.
\end{aligned}
\qquad (32)
$$

Now, consider the following two models

$$\dot{v}_{min} = \Phi_{min}(v_{min}), \quad \dot{v}_{max} = \Phi_{max}(v_{max}). \qquad (33)$$

From the Comparison Lemma [14], for all $v_{in}(t) > 0$,

$$v_{min}(t) \le v_{in}(t) \le v_{max}(t).$$

For all $v_{min}(0) > v_{min}^1$, $v_{min}(t)$ remains positive and converges to v_{min}^2. In the same way, for all $v_{max}(0) > 0$, $v_{max}(t)$ stays positive and converges to v_{max}^1. This proves P2. This also shows that v_{in} only takes strictly positive values, i.e., it is never zero, which in turn proves that u_b is bounded. Therefore, there exist free parameters satisfying (27). ∎

The physical interpretation of the boundedness of v_o and v_{in} as proved above can be explained as follows. With I_b bounded, the output power $p_o = v_l I_b - r_o I_b^2 = v_o I_b$ is bounded and, thus, v_o is also bounded. Since the converter is a passive device, it follows that the input power $p_{in} = \frac{v_b - v_{in}}{r_{in}}v_{in}$ is bounded and, thus, v_{in} is also bounded.

The controller implementation diagram is shown in Fig. 6. Notice that, to calculate I_b^r, measurements of currents I_{dab} and I_b are required. As mentioned, the signal I_b^r is passed through a low-pass filter to eliminate noise. The phase shift then follows from (26). Also, bounds (27) in Proposition 1 imply that by choosing appropriately the system parameters n_b, L_b and f_b, the control input ϕ_b can be ensured to be unsaturated. The parameters can be chosen by the designer to enhance the transient performance of the battery states.

C. Stability of the n-SST System

We next extend the stability proof to a n-SST network where $n \ge 1$. Following standard assumptions as in [15], we neglect the effect of the second harmonics on the dynamics of v_{fi} in (3) as their impact on the steady-state value of
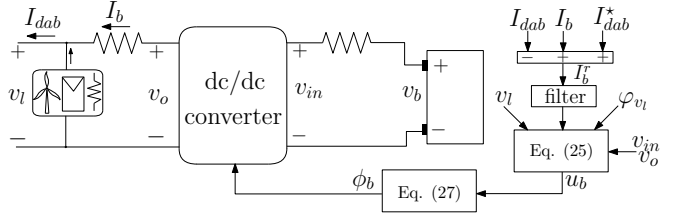
(3) is small from small-ripple approximation. Since we are primarily interested in the fundamental frequency response, the v_{fi}-dynamics is approximated to

$$\dot{v}_{fi} = -\frac{v_{fi} - v_{hi}}{C_{fi}} - \frac{1}{2C_{fi}}(d_{1i}i_{di} + d_{2i}i_{qi}). \qquad (34)$$

Using (22) and the definition of δ, we rewrite (12) in the equivalent form

$$\dot{v}_{li} = \frac{n_{si}\phi_{si}(1 - \phi_{si})}{2C_{li}f_{si}L_{si}}v_{li} - \frac{I_{dabi}^\star}{C_{li}} - \frac{\delta_i}{C_{li}}. \qquad (35)$$

The closed-loop is then conformed by equations (1), (2), (34), (4)-(6), (11), (35) and (28)-(29). A block diagram representation is showed in Fig. 7. As it can be seen, the closed-loop admits a (double) cascade representation. The cascaded system $\Sigma_1 - \Sigma_2$ is given by

$$
\begin{bmatrix} \dot{z} \\ \dot{\tilde{I}}_b \end{bmatrix} = \begin{bmatrix} \gamma(z, \alpha_c) \\ K_p\tilde{I}_b \end{bmatrix} + \begin{bmatrix} P \\ 0 \end{bmatrix} \tilde{I}_b
\qquad (36)
$$

where the function $\gamma : \mathbb{R}^{9n} \to \mathbb{R}^{9n}$ accounts for the nonlinearities of the rectifier, DAB converter and controllers dynamics. Also, $z^\top = [z_1^\top \cdots z_n^\top] \in \mathbb{R}^{9n}$. The constant vector $\alpha_c \in \mathbb{R}^{8n}$ contains the controller gains. The subvectors $z_i^\top = [x_i^\top \ \xi_{1i} \ \cdots \ \xi_{4i}]$ with $x_i^\top = [i_{di} \ i_{qi} \ v_{fi} \ v_{hi} \ v_{li}]$. We define vector $\tilde{I}_b^\top = [\delta_1 \ \cdots \ \delta_n] \in \mathbb{R}^n$, and constant matrices $P = [-\frac{1}{C_{f1}}v_5 \ \cdots \ -\frac{1}{C_{fn}}v_{(9n-4)}] \in \mathbb{R}^{9n \times n}$ and $K_p = \mathrm{diag}(-\frac{\kappa_{p1}}{r_{o1}C_{on}}, \cdots, -\frac{\kappa_{pn}}{r_{on}C_{on}}) \in \mathbb{R}^{n \times n}$. We have denoted by $v_j \in \mathbb{R}^{9n}$ a vector of the Euclidean basis with its jth-element equal to one. The linearized state model of (36) can be the written as

$$
\begin{bmatrix} \dot{\delta z} \\ \dot{\tilde{I}}_b \end{bmatrix} = \begin{bmatrix} \Gamma(\alpha_c) & P \\ 0 & K_p \end{bmatrix} \begin{bmatrix} \delta z \\ \tilde{I}_b \end{bmatrix}
\qquad (37)
$$

where $\Gamma \in \mathbb{R}^{9n \times 9n}$ is

$$\Gamma = \frac{\partial\gamma(z)}{\partial z}\Big|_{z=z_\star},$$

with $z_\star$ the equilibrium point of (1)-(17) for $i = 1, \cdots, n$. Note that the eigenvalues of (37) are $\mathrm{eig}\{\Gamma\} \cup \{-\frac{\kappa_{p1}}{r_{o1}C_{o1}}, \cdots, -\frac{\kappa_{pn}}{r_{on}C_{on}}\}$. Thus, if every PI gain (i.e., vector α_c) is selected such that $\mathrm{Re}[\mathrm{eig}\{\Gamma\}] < 0$, then the closed-loop system of interconnected n SST-driven microgrids (1)-(17) will be locally asymptotically stable.

Block Σ_3 in Fig. 7 corresponds to the v_{ini}-dynamics $(i = 1, \cdots, n)$ introduced in (29). From stability of the cascade $\Sigma_1 - \Sigma_2$, it follows that functions p_i, the inputs of Block Σ_3, are bounded. The later validates Assumption 2 and Proposition 1. Thus, the overall closed-loop system is stable.
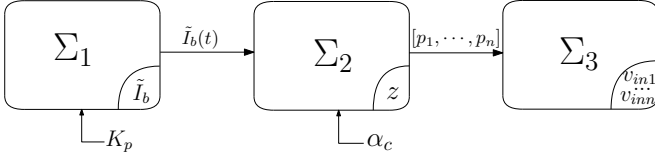
Fig. 7: Cascade representation of the closed-loop system.

IV. MULTI-SST POWER SHARING

Change in load currents can be categorized into two scenarios. The first scenario is when the change is small enough that $|I_b^r| \leq I_b^{max}$, i.e., the battery current magnitude of I_b^r needed for the slack is less than the maximum capacity of the battery. In this case, the SST whose load changed can compensate for the deficit power locally using the decentralized controller (17), as described in Section III. However, if the load change is so high that $|I_b^r| \geq I_b^{max}$, then other SSTs in the network need to be used to support the deficit. The control action will still remain decentralized as in section III, but the computation of the voltage and current setpoints for the mth SST (i.e., the SST whose load changed) will now depend on the neighboring SSTs. The way to implement this can be as follows. First, the inability of the mth SST in supporting its new load is detected, and immediately after the setpoints $P_{reci}^\star$ of every SST, $i = 1, .., n$, are overwritten to enable power sharing. Subsequently, the corresponding currents setpoints $I_{dabi}^\star$ are updated according to (19). For any iteration, $P_{reci}^\star$ must satisfy the power balance equation—for details on this equation, please see [16]

$$\left(i_{di}^\star + \frac{v_{di}^\star}{2r_{fi}}\right)^2 + \left(i_{qi}^\star + \frac{v_{qi}^\star}{2r_{fi}}\right)^2 = \frac{v_{di}^{\star 2} + v_{qi}^{\star 2}}{4r_{fi}^2} - \frac{2P_{reci}^\star}{r_{fi}}. \tag{38}$$

Any change in $i_{di}^\star$ or $v_{di}^\star$ in one of the SST in the network will also impact the others. In order to avoid this complexity power sharing methods for SST systems developed in our previous work [16] are utilized in a cooperative multi-SST context. These algorithms allow to properly update $i_{di}^\star, i_{qi}^\star, v_{di}^\star$ and $v_{qi}^\star$. They are summarized below.

A. Method 1: Constant Current Method

In this method, when there is a load change in the mth SST that cannot be supported by its local storage, the other SSTs assist without changing its input current. That means that for all $i \neq m$, the currents $i_{di}^\star$ and $i_{qi}^\star$ remain unaltered. The input voltage of all the SSTs is updated to a new value as a function of the change in power. The analytical expressions for the change of the input current of the mth SST can be expressed as

$$\left(r_{fm} + \sum_{k=1}^{m} r_k\right)\Delta i_{dm}^{\star 2} + \left(2r_{fm}i_{dm}^\star + v_{dm}^\star + \sum_{k=1}^{i} r_k i_{dm}^\star \right.$$
$$\left. + \sum_{k=1}^{i} x_k i_{qm}^\star\right)\Delta i_{dm} + 2\Delta P_{recm} = 0. \tag{39}$$

Algorithm 1 Constant current method

---
while $I_{bm}^r = I_{bm}^{max}$ **do**
  if $\delta_m > 0$ **then**
    $P_{recm} \leftarrow$ Calculate the updated power requirement based on equation (19).
    if $P_{recm} \leq P_{recm}^{max}$ **then**
      $P_{recm}^\star \leftarrow P_{reci}$
    else
      $P_{recm}^\star \leftarrow P_{recm}^{max}$
    end if
    $i_{dm}, v_{dm} \leftarrow$ Update following equation (38) for the mth SST
    $v_{di} \leftarrow$ Update following Power Sharing Method 1; $i = 1 \rightarrow n, i \neq m$
    $P_{reci} \leftarrow$ Update using equation (39) for the ith SSTs
    if $P_{reci} \leq P_{reci}^{max}$ **then**
      $P_{reci}^\star \leftarrow P_{reci}$
    else
      $P_{reci}^\star \leftarrow$ Continue the IEM command
      $P_{recm}^\star \leftarrow$ Continue the IEM command
    end if
  end if
end while

Keeping $i_{qm}^\star$ unchanged, the current change $\Delta i_{dm}^\star$ of the mth SST is the root of (39). Also, the voltage relation follows as

$$\Delta v_{dm} + j\Delta v_{qm} = (\Delta i_{dm} + j\Delta i_{qm})\sum_{k=1}^{m}(r_k + jx_k).$$

The voltage drop at all other SSTs in the network will be the same as that of the mth SST to maintain the input current as it is. Algorithm 1 shows step by step execution of Method 1 to update the new power setpoints in a radial network. Once the power setpoints $P_{reci}^\star$ are updated, $I_{dabi}^\star$ is recalculated as in equation (19). The battery current is then regulated with the designed local controller in Section III with updated $I_{dabi}^\star$.

B. Method 2: Constant Voltage Method

The second method maintains feasible operation through constant node voltage of all other SSTs when there is any change in the mth SST. Because of the radial configuration, only the input current references of the immediate neighboring SSTs: $(m-1)^{th}$ and $(m+1)^{th}$ SST change whereas the other setpoints remain invariant [16]. Algorithm 2 shows step by step execution of method 2 to update the power setpoints of the neighboring SSTs in a radial network. Once the power setpoints $P_{reci}^\star$ are updated for the neighbors, $I_{dabi}^\star$ are recalculated as in equation (19) and battery current is subsequently regulated with the designed local controller in Section III following updated $I_{dabi}^\star$. Note that in this method, only the immediate neighbors share the load which may not be practical for a big change in the load power. This method is thus more suitable for smaller-scale microgrid networks where every SST may not have storage.

V. SIMULATION RESULTS

The proposed controller and power sharing methods are next validated using simulations on a radial 9-bus distribution feeder model containing one SST at each bus. The tie-line

Algorithm 2 Constant voltage method

---

while $I_{bm}^r = I_{bm}^{max}$ **do**
  if $\delta_m > 0$ **then**
    $P_{recm} \leftarrow$ Calculate the updated power requirement based on equation (19).
    if $P_{recm} \leq P_{recm}^{max}$ **then**
      $P_{recm}^* \leftarrow P_{recm}$
    else
      $P_{recm}^* \leftarrow P_{recm}^{max}$
    end if
    $i_{dm}, v_{dm} \leftarrow$ Update following equation (39) for m^{th} SST
    $i_{di} \leftarrow$ Update following Power Sharing Method 2; $i = (m-1), (m+1)$
    $P_{reci} \leftarrow$ Update using equation (38) for i^{th} SSTs
    if $P_{reci} \leq P_{reci}^{max}$ **then**
      $P_{reci}^* \leftarrow P_{reci}$
    else
      $P_{reci}^* \leftarrow$ Continue the IEM command
      $P_{recm}^* \leftarrow$ Continue the IEM command
    end if
  end if
end while

Fig. 8: Storage current profile with change in net loads.

impedances of this model, which are based on the IEEE 34-bus distribution system, are: $Z_{01} = 0.653 + j0.651$, $Z_{12} = 0.438 + j0.437$, $Z_{23} = 8.16 + j8.14$, $Z_{34} = 9.49 + j9.47$, $Z_{45} = 7.53 + j7.51$, $Z_{56} = 0.0037 + j0.0027$, $Z_{56} = 0.0037 + j0.0027$, $Z_{67} = 0.906 + j0.481$, $Z_{78} = 25.52 + j13.546$, $Z_{89} = 7.284 + j13.865$. The SST models are identical and their parameters are based on the GEN-II SST model [17]. First, results are provided to validate the control with added stochastic randomness to the loads and current sources representing the wind and solar energy. Then, the designed controller is utilized to apply Method 1 in case of a sudden change in the load when the local storage is not capable to support the change. The latter is extended to the case when there exist delays in the computation of the setpoint updates. To avoid redundancy, closed-loop responses of only SST1 through SST3 are displayed in each figure.

A. Autonomous operation: $|I_b^r| \leq I_b^{max}$

The simulation starts with a nominal load of 1 kW at time $t = 0$ in SST1 and SST3 to SST7. SST2 starts with 10 kW and SST8 and SST9 with -1 kW. Load and renewable generation are changed in all the SSTs except for SST3, SST5, SST7 and SST9. The storage response to the dynamic I_b^r is observed in Fig. 8 for SST1-SST3. Similar responses were observed for SST4-SST9 as well. It is found for all the SSTs, the storage current accurately follows the reference (dotted line) for any changes in the load (as long as $I_b^r \leq I_b^{max}$) with the developed controller. $I_b^{max} = 50$ A for simulation validation. The net load is varied from 0 A to 10 A by controlling PV current level and load demands. When there is no change in the net load then I_b^r remains as unchanged.

B. Power Sharing operation: $|I_b^r| > I_b^{max}$

The wind and PV currents are kept constant for all the SSTs before $t_0 = 0.6$ s. Power setpoints P_{reci}^* are shown in
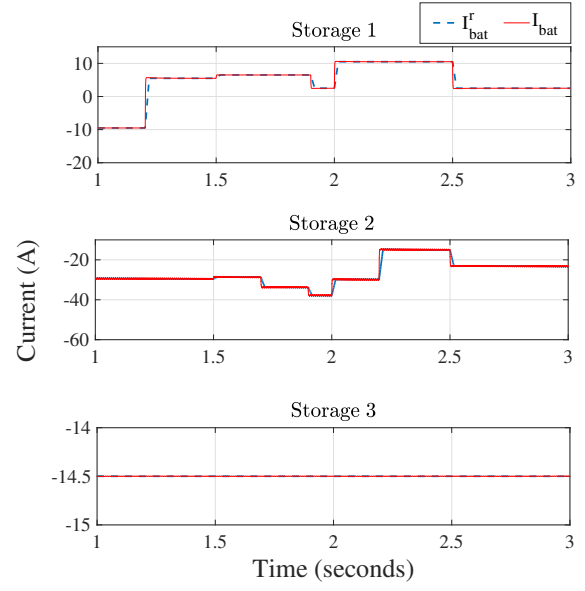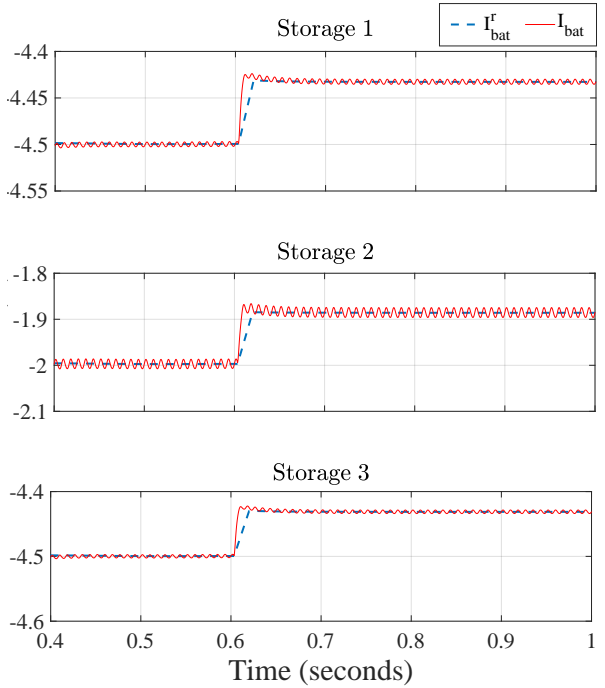

Fig. 9: Storage current profiles when sharing power after a change in net load in SST1.

Table II. Afterwards, a sudden load change of 0.5 kW in the net power happens at $t_0 = 0.6$ s in SST5 which drives the magnitude of I_b^r to exceed I_b^{max} set at 12 A. Subsequently, I_b^r gets updated for all the SSTs and I_b follows as shown in Fig. 9. The ripples present in the response of I_b is due to the second harmonics of the rectifier output voltage (3) that also impact the output voltage v_l because of the battery
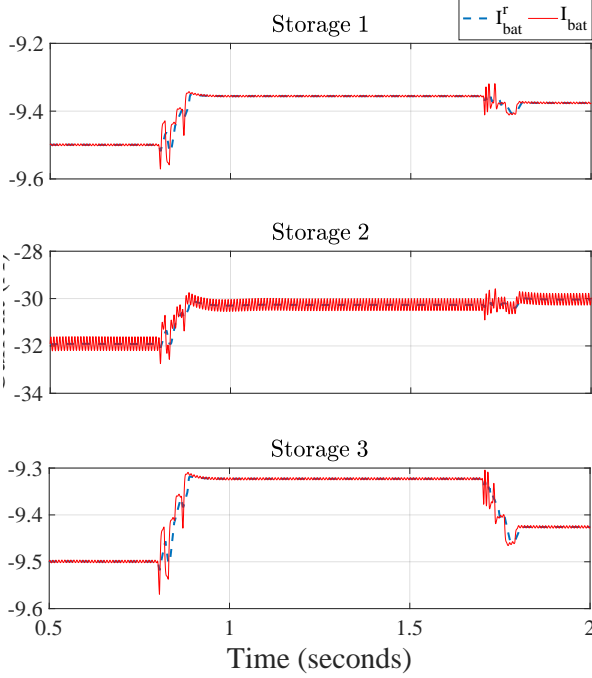
Fig. 10: Storage current profile when sharing power delay after a change in net load in SST1.

TABLE II: Power setpoints before/after the load change (kW).

SST#	$P_{rec}^{\star}(t < t_0)$	$P_{rec}^{\star}(t \geq t_0)$	
		Method 1	Method 2
1, 3, 8, 9	-1	-1.027	-1
2	-2	-2.044	-2
4	1	1.06	0.95
5	1	-0.6	-0.6
6	1	1.06	2.53
7	1	1.06	1

interface into the DC bus. However, the ripples are very small in magnitude and within a range of $0.001\% - 0.005\%$. The setpoint calculation for power sharing is almost instantaneous, and hence the control is actuated immediately once the new setpoints are calculated. The convergence times for the closed-loop response of the SST currents is around 0.05 s. To compare Method 1 with 2, Table II shows the new setpoints $P_{rec}^{\star}(t \geq t_0)$ calculated with both algorithms. As seen from the table, in method 1, all the SSTs update their setpoint along with grid to support SST5. On the other hand, in method 2, only its immediate neighbors compensate the load changes. It is important to mention that grid current remains unchanged in Method 2 as the change in power is fully compensated by its neighbors.

Finally, we simulate a scenario in which the operation points are not updated immediately after the load change. This is intended to emulate the computational delay that exists while updating the new setpoints. The results are shown in Fig. 10. Oscillations are observed as the SSTs

operate under wrong setpoints. However, as the setpoins and I_b^r are updated within 0.01 s, the system reaches a new steady state within 0.05 s.

VI. CONCLUSION

This paper developed a nonlinear control framework for controlling storage devices in networked microgrids considering the intermittent behavior of renewable energy sources and loads. Special attention is paid to the nonlinear dynamics of both the microgrid model and the storage model for designing this controller, and guaranteeing closed-loop stability. The controller can be implemented in a completely decentralized way using local output feedback only. Results are verified using IEEE prototype distribution feeder models. The proposed approach can be particularly important for power sharing among microgrids during storms and natural calamities, when power from healthy parts of the network need to be transfered to other remote parts in a stable way. Future work along this direction will include extension of these results under various cyber-physical uncertainties in SST-to-SST communication, and also evaluating the impact of malicious cyber intrusions (such as misleading manipulations in the SST setpoints) on closed-loop stability.

REFERENCES

[1] J. M. Guerrero, J. C. Vasquez, J. Matas, L. G. de Vicuna, and M. Castilla, "Hierarchical control of droop-controlled AC and DC microgrids—A general approach toward standardization," *IEEE Transactions on Industrial Electronics*, vol. 58, no. 1, pp. 158–172, Jan 2011.

[2] D. E. Olivares, A. Mehrizi-Sani, A. H. Etemadi, C. A. Cañizares, R. Iravani, M. Kazerani, A. H. Hajimiragha, O. Gomis-Bellmunt, M. Saeedifard, R. Palma-Behnke, G. A. Jimnez-Estevez, and N. D. Hatziargyriou, "Trends in microgrid control," *IEEE Transactions on Smart Grid*, vol. 5, no. 4, pp. 1905–1919, 2014.

[3] A. Q. Huang, M. L. Crow, G. T. Heydt, J. P. Zheng, and S. J. Dale, "The future renewable electric energy delivery and management (freedm) system: The energy internet," *Proceedings of the IEEE*, vol. 99, no. 1, pp. 133–148, 2011.

[4] G. Parise, L. Martirano, M. Kermani, and M. Kermani, "Designing a power control strategy in a microgrid using PID / fuzzy controller based on battery energy storage," in *IEEE International Conference on Environment and Electrical Engineering and IEEE Industrial and Commercial Power Systems Europe*, 2017, pp. 1–5.

[5] M. C. Such and G. Y. Masada, "BESS control on an microgrid with significant wind generation," in *IEEE Power Energy Society General Meeting*, July 2017, pp. 1–5.

[6] R. K. Sharma and S. Mishra, "Dynamic power management and control of a PV PEM fuel-cell-based standalone AC/DC microgrid using hybrid energy storage," *IEEE Transactions on Industry Applications*, vol. 54, no. 1, pp. 526–538, 2018.

[7] A. Egea-Alvarez, J. Berteen, D. Van Hertem, and O. Gomis-Bellmut, "Hierarchical power control of multiterminal hvdc grids," *Electric Power Systems Research*, vol. 121, pp. 207–215, 2015.

[8] G. G. Karady, A. Q. Huang, and M. Baran, "FREEDM system: An electronic smart distribution grid for the future," *IEEE Transmission and Distribution Conference and Exposition*, pp. 1–6, 2012.

[9] M. T. A. Khan, A. A. Milani, A. Chakrabortty, and I. Husain, "Dynamic modeling and feasibility analysis of a solid-state transformer based power distribution system," *IEEE Transactions on Industry Applications*, vol. 54, no. 1, pp. 551–562, 2018.

[10] H. Bai and C. Mi, "Eliminate reactive power and increase system efficiency of isolated bidirectional dual-active-bridge DC-DC converters using novel dual-phase-shift control," *IEEE Transactions on Power Electronics*, vol. 23, no. 6, pp. 2905–2914, 2008.

[11] ——, "Correction to "eliminate reactive power and increase system efficiency of isolated bidirectional dual-active-bridge DC-DC converters using novel dual-phase-shift control"," *IEEE Transactions on Power Electronics*, vol. 27, no. 9, pp. 4177–4177, 2012.

[12] M. Chen and G. A. Rincon-Mora, "Accurate electrical battery model capable of predicting runtime and I−V performance," *IEEE Transactions on Energy Conversion*, vol. 21, no. 2, pp. 504–511, 2006.

[13] A. Isidori, *Nonlinear Control Systems*.   Springer, 1995.

[14] H. Khalil, *Nonlinear Control*.   Pearson, 2015.

[15] R. W. Erickson and D. Maksimovic, *Fundamentals of Power Electronics*.   Springer, 2001.

[16] A. A. Milani, M. T. A. Khan, A. Chakrabortty, and I. Husain, "Equilibrium point analysis and power sharing methods for distribution systems driven by solid-state transformers," *IEEE Transactions on Power Systems*, vol. 33, no. 2, pp. 1473–1483, 2018.

[17] F. Wang, G. Wang, A. Huang, W. Yu, and X. Ni, "Design and operation of a 3.6kV high performance solid state transformer based on 13kv SiC MOSFET and JBS diode," in *IEEE Energy Conversion Congress and Exposition*, 2014, pp. 4553–4560.